Supersolid Phases of Bosonic Particles in a Bubble Trap

Matteo Ciardi,[1,2,3,*] Fabio Cinti,[1,3,4,†] Giuseppe Pellicane,[5–8,‡] and Santi Prestipino[9,§]

[1]Dipartimento di Fisica e Astronomia, Università di Firenze, I-50019 Sesto Fiorentino (FI), Italy
[2]Institute for Theoretical Physics, TU Wien, Wiedner Hauptstraße 8-10/136, 1040 Vienna, Austria
[3]INFN, Sezione di Firenze, I-50019 Sesto Fiorentino (FI), Italy
[4]Department of Physics, University of Johannesburg, P.O. Box 524, Auckland Park 2006, South Africa
[5]Dipartimento di Scienze Biomediche, Odontoiatriche e delle Immagini Morfologiche e Funzionali, Università degli Studi di Messina, I-98125 Messina, Italy
[6]CNR-IPCF, Viale F. Stagno d'Alcontres, 37-98158, Messina, Italy
[7]School of Chemistry and Physics, University of Kwazulu-Natal, 3209 Pietermaritzburg, South Africa
[8]National Institute of Theoretical and Computational Sciences (NIThECS), 3209 Pietermaritzburg, South Africa
[9]Dipartimento di Scienze Matematiche e Informatiche, Scienze Fisiche e Scienze della Terra, Università degli Studi di Messina, viale F. Stagno d'Alcontres 31, I-98166 Messina, Italy

(Received 10 March 2023; revised 6 June 2023; accepted 4 December 2023; published 8 January 2024)

Confinement can have a considerable effect on the behavior of particle systems and is therefore an effective way to discover new phenomena. A notable example is a system of identical bosons at low temperature under an external field mimicking an isotropic bubble trap, which constrains the particles to a portion of space close to a spherical surface. Using path integral Monte Carlo simulations, we examine the spatial structure and superfluid fraction in two emblematic cases. First, we look at soft-core bosons, finding the existence of supersolid cluster arrangements with polyhedral symmetry; we show how different numbers of clusters are stabilized depending on the trap radius and the particle mass, and we characterize the temperature behavior of the cluster phases. A detailed comparison with the behavior of classical soft-core particles is provided too. Then, we examine the case, of more immediate experimental interest, of a dipolar condensate on the sphere, demonstrating how a quasi-one-dimensional supersolid of clusters is formed on a great circle for realistic values of density and interaction parameters. Crucially, this supersolid phase is only slightly disturbed by gravity. We argue that the predicted phases can be revealed in magnetic traps with spherical-shell geometry, possibly even in a lab on Earth. Our results pave the way for future simulation studies of correlated quantum systems in curved geometries.

DOI: 10.1103/PhysRevLett.132.026001

Computing the equilibrium properties of quantum many-body systems remains a main objective of contemporary physics. In this respect, ultracold atoms provide a framework where geometry and interactions can be tuned almost at will, allowing one to test fundamental many-body theories [1,2]. A system of atoms (loosely) confined to an ellipsoidal surface [3,4] represents a typology that only recently has started to be explored. To achieve this goal, a quantum gas is loaded into a shell trap, where atoms are subject to a quadrupolar field "dressed" by a radio frequency (rf) field [5–9]. In the limit of slow atomic motion in a strong magnetic field, the effective potentials of the internal states are the position-dependent eigenvalues of the Hamiltonian consisting of the bare potentials and the coupling term [10]. For atoms in the upper dressed state, resonance is reached at the surface of an ellipsoid. However, to let atoms explore the full surface, experiments must be performed in outer space [11–13] or adopt some gravity compensation mechanism [14,15]. Coherent and isotropic shells of atoms slowly expanding in microgravity can be generated too [16].

The realization of shell-shaped condensates has fueled a renewed interest in the problem of quantum particles in curved geometries [17], and particularly in the quantum phases that free and interacting bosons can exhibit. Several recent works have investigated Bose-Einstein condensation as well as the superfluid-to-normal fluid transition on a sphere [18–22], while others have studied the dynamics and thermodynamics of the condensate itself [23–26]. Most of these works have considered weakly interacting particles, although some have looked into the condensed phases arising from dipolar interactions [26–29].

While experiments have so far been performed in the same dilute limit, bubble traps open the exciting prospect of investigating the physics of strongly correlated quantum particles in curved spaces, with all the advantages brought by ultracold-atom setups. For example, ultracold atoms may serve as quantum simulators to test fundamental physics; therefore, studying the effects of curvature in a controlled environment can be of interest to other fields ranging from cosmology to biology [30,31]. Similarly, we

can envisage the possibility to control the self-assembly of a many-body system through a convenient choice of the confining surface, i.e., of the shape of the ensuing geometric potential [17]. Equally important is to figure out experiments on curved many-body systems that could be accomplished on Earth, i.e., without the necessity of compensating gravity [32]. In this respect, the most awaited developments concern dipolar atoms [33], which have already been examined in flat space and harmonic traps [34,35] and are known to give rise to supersolid phases [36–39]. At the same time, it will be interesting to see whether the confined geometry of bubble traps can stabilize the supersolid phase in small systems of Rydberg-dressed atoms [40–44].

In this Letter, we use the path integral Monte Carlo (PIMC) simulation method to give a first glimpse of the equilibrium phases that can arise in a shell-trapped system of identical bosonic particles. In particular, we will provide the first compelling evidence of supersolid order for two distinct instances of the interaction potential. First, we look at the penetrable-sphere model as an example of soft-core potential and a paradigmatic interaction in condensed matter physics that gives rise to both superfluidity and clusterization [45–48]; for this interaction, we compare our results with various benchmarks. Then, we investigate the effects of a dipole-dipole interaction, more closely related to experiments, and we show, for a realistic choice of parameters, that a supersolid cluster phase indeed occurs in shell geometry. Remarkably, this supersolid is resistant to the gravity of Earth.

To keep contact with the experiments, we simulate spinless bosons in three-dimensional space under the constraint of an external potential analogous to that realized in the lab. For N particles with mass m, the Hamiltonian reads

$$H = \sum_{i=1}^{N} (-\lambda \nabla_{\mathbf{r}_i}^2 + u_{\mathrm{ext}}(|\mathbf{r}_i|)) + \sum_{i<j} v_{\mathrm{int}}(\mathbf{r}_i - \mathbf{r}_j), \quad (1)$$

where $\mathbf{r}_i$ is the position of the ith particle, $\lambda = \hbar^2/2m$, v_{int} is the (possibly anisotropic) interaction potential, and

$$u_{\mathrm{ext}}(d) = (u_0/\Omega)\sqrt{(d^2 - \Delta)^2/4 + \Omega^2} - u_0 \quad (2)$$

is the external potential appropriate to a spherically symmetric bubble trap [24] centered at the origin. In Eq. (2), Δ and Ω are square-length parameters related to the detuning and Rabi frequency of the rf field, respectively, while u_0 characterizes the harmonic trap prior to dressing. The potential (2) interpolates between the filled sphere and the spherical shell [see Fig. 1(g)]. In the thin-shell limit, u_{ext} becomes harmonic around the minimum at $\sqrt{\Delta}$, which thus defines the radius R of the reference sphere. As R increases, the potential minimum gets more and more pronounced, until particles become effectively confined to a spherical surface.

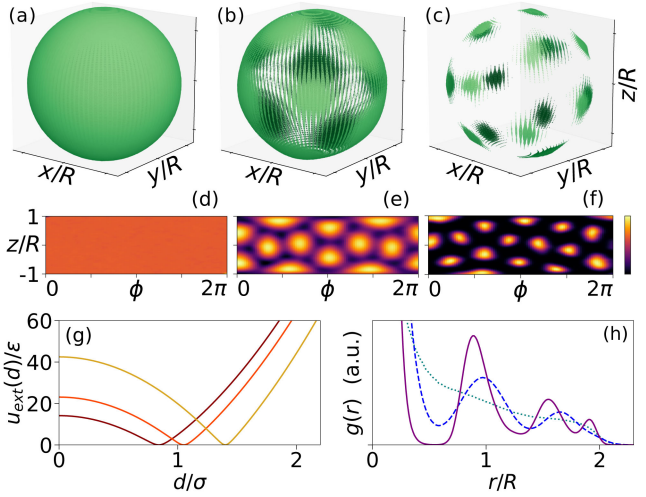

FIG. 1. Soft-core bosons in an isotropic bubble trap. (a)–(c) Particle density for $N = 120$, $T = 0.125$, $R = 1.4$, $u_0 = 2$, $\Omega = 0.0441$, and $\lambda = 0.5$ (a), 0.16 (b), 0.01 (c). The size of the points is proportional to the density averaged along the radial direction, and the shading is a guide for the eye: Brighter points are closer to the observer. (d)–(f) Area-preserving projections of the densities in (a)–(c). Brighter colors indicate a larger density (log scale). (g) External potential (2) for $u_0 = 2$, $\Omega = 0.0441$, and $R = 0.84$ (brown), 1.05 (red), and 1.4 (gold). (h) Pair distribution function for the same parameters in (a)–(c): $\lambda = 0.5$ (blue dotted line), 0.16 (blue dashed line), 0.01 (purple solid line).

In our PIMC simulations [49], we employ the worm algorithm [50] to sample the equilibrium statistics of bosons at finite temperature and estimate the superfluid fraction, f_s [51]. To deal with the strong spatial constraint due to (2), we introduce a biased version of the PIMC method [51]. We also perform classical Monte Carlo (MC) and molecular dynamics (MD) simulations to probe the classical limit in the soft-core case.

We begin by considering bosons interacting through the soft-core potential:

$$v_{\mathrm{int}}(\mathbf{r}) = \epsilon\theta(\sigma - r), \quad (3)$$

where $\epsilon > 0$, and σ is the core diameter. In the discussion of the soft-core model, ϵ and σ are taken as units of energy and length, respectively; temperatures are expressed in units of ϵ/k_B. Because of the peculiar nature of the repulsion, at high density particles are gathered in droplets or clusters [77]. Employing mean-field theory at $T = 0$, the authors of Ref. [78] explored various possible arrangements of clusters on the sphere, finding the configuration of lowest enthalpy as a function of the radius. The evidence of supersolid phases is, however, not conclusive: Condensation of clusters is assumed, not derived, while there is no guarantee that the true ground state has been identified. Using, for the first time, *ab initio* PIMC simulations, we provide for the

same interaction (3) conclusive evidence of supersolid order. Moreover, we show how the supersolid withstands finite temperature in a realistic bubble trap, i.e., beyond a purely two-dimensional setup.

First, we investigate the behavior of the system at a temperature $T \ll 1$, choosing $\Omega = 0.0441$ (an arbitrary value much smaller than Δ; see below). In Figs. 1(a)–1(f), we give a graphical account of the structures found for decreasing λ at $T = 0.125$, which are indicative of a superfluid-supersolid-insulator "transition," similar to what occurs on a plane [79]. Specifically, we perform a size scaling analysis of f_s at fixed $N/(4\pi R^2) = 4.87$ for two strengths of the trap potential to see how the system approaches the planar limit. On a plane, the phases were characterized in terms of the dimensionless interaction strength $\alpha = m\rho\sigma^4\epsilon/\hbar^2 = \rho\sigma^4\epsilon/(2\lambda)$ (for a number density $\rho = 4.4$), finding that the superfluid-supersolid transition occurs at $\alpha \approx 13$, whereas the system becomes insulating at $\alpha \approx 22$ [79]. In both two and three dimensions, the former transition is marked by a jump in f_s [45]. Our results are reported in Fig. 2. In the strongly confined case ($u_0 = 50$, top panel), the planar behavior is already recovered for $N = 120$ particles, while for smaller sizes we find a smooth crossover. For a weaker external potential ($u_0 = 2$, bottom panel), the transition to supersolid is milder and shifted toward higher α values; moreover, convergence to the planar limit is much slower. In both cases, the system is a density wave at large α; as α is reduced, quantum fluctuations increase, eventually leading to a disruption of polyhedral order which is faster when more freedom is given to particles in the radial direction, i.e., for $u_0 = 2$. The same sequence of transitions is reflected in the shape of the pair distribution function $g(r)$ [see Fig. 1(h) and [51]]. As long as $f_s > 0$, $g(r)$ is nonzero at any distance, which is consistent with a condensate wave function being nonzero everywhere on the sphere. Instead, in a normal solid near zero temperature, $g(r)$ would ideally be zero in the interstitial region between two successive shells of neighbors. The deviations from this behavior at moderate to large distances are a temperature effect, ultimately due to the finite extension of the clusters.

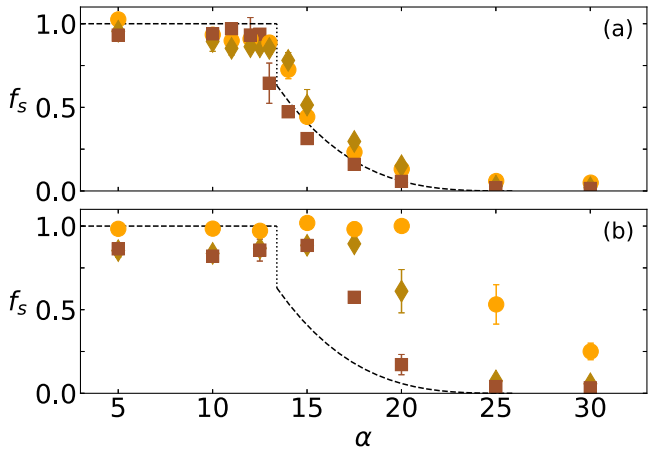

FIG. 2. Superfluid fraction across the superfluid-supersolid-insulator transition plotted as a function of α for $T = 0.125$ [the ρ entering the expression of α is $N/(4\pi R^2)$]. (a) $u_0 = 50$. (b) $u_0 = 2$. Different symbols correspond to different system sizes: $N = 40$ and $R = 0.808$ (circles), $N = 80$ and $R = 1.143$ (diamonds), $N = 120$ and $R = 1.4$ (squares). The dashed lines refer to the planar limit [80].

Next, we fix the number N of particles (120) and the temperature T (0.5), and set $u_0 = 2$ and $\Omega = 0.0441$ [we require $\Omega \ll 1$, so as to have $u_{\rm ext}(0) \approx \Delta/\Omega \gg 1$ for $R \approx 1$]. We collect in a diagram the equilibrium arrangements for various λ and R [Fig. 3(a)]. On account of the f_s value and the evidence or not of polyhedral order, we can reasonably distinguish between superfluid, supersolid, and normal-solid states. Throughout the "solid" regions, the number N_c of clusters may vary, but clusters are invariably found at the vertices of a regular or semiregular polyhedron: for example, an octahedron for $N_c = 6$, a square antiprism for $N_c = 8$, and an icosahedron for $N_c = 12$ [51]. For some (λ, R) pairs, the cluster structure agrees with those predicted in [78] (for example, the icosahedral structure at $\lambda = 0.16$ and $R = 1.4$). However, for several other pairs, the equilibrium configuration is a novel cluster phase not seen before. Moreover, contrary to the mean-field prediction, we see that decreasing λ at fixed R leads to

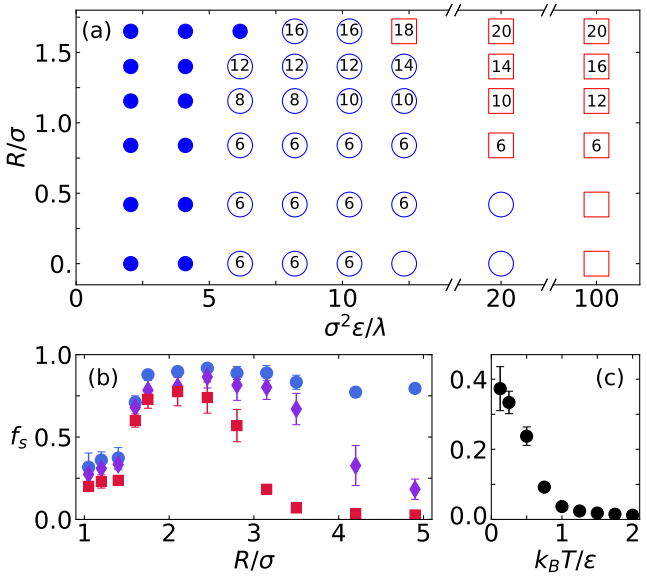

FIG. 3. (a) A diagram showing for $N = 120$ and $T = 0.5$ the number N_c of clusters as a function of λ^{-1} and R. The blue dots are state points where the system is superfluid. Open circles and squares mark supersolid and normal-solid states, respectively. When λ and R are both small, N_c depends on the initial conditions (see more in [51]); therefore, no number is printed in the symbol. (b) Superfluid fraction f_s plotted as a function of R at fixed $\lambda = 0.16$ and $u_0 = 50$ for $T = 0.5$ (red squares), 0.25 (purple diamonds), and 0.125 (blue circles). (c) T dependence of f_s for $R = 1.4$ and $\lambda = 0.16$.

transitions between equilibrium configurations with different numbers of clusters. As we increase the radius, the supersolid region shrinks, while the number of clusters grows. At large radii, the particles assemble in smaller clusters, making it more difficult for the system to sustain superfluidity; eventually, above a certain R the system is so dilute that clusters are washed away for every λ.

In the $T \to 0$ limit, the superfluid phase is stable at all large radii. Upon heating, similar to flat space, a superfluid-to-normal-fluid transition eventually occurs. This is illustrated for $\lambda = 0.16$ in Fig. 3(b), where we plot the superfluid fraction as a function of R at different temperatures. As T goes up, f_s is gradually reduced until it vanishes, starting from larger R values. At high enough temperatures, f_s is also depleted for the supersolid, as we show in Fig. 3(c) for $R = 1.4$ and $\lambda = 0.16$: Interestingly, however, polyhedral order is preserved throughout the range of temperatures.

When $\lambda \to 0$, the number of clusters approaches a value dependent on R; this regime corresponds to the classical limit, regardless of R and $T > 0$. To make sure that this is indeed the case, we have considered the classical counterpart of the quantum problem. The first observation of cluster phases in classical particles on a sphere goes back to Ref. [81], where density-functional-theory calculations are presented. Here, to keep the same level of accuracy of the quantum treatment, we carry out extensive MC and MD simulations of classical soft-core particles, using the same parameters of the quantum simulations. The results expressed in terms of the number and final arrangement of clusters are reported in [51] for various R values. Except for small radii, where the uncertainty in N_c is large, the aggregates formed by quantum particles have a comparatively smaller number of clusters. This is an effect of quantum delocalization, which causes the effective diameter of bosons to be larger than σ.

We now move to examine the behavior of dipolar bosons in the thin-shell limit. As is common in experiments, we assume atoms to be polarized along $\hat{\mathbf{z}}$. We work with a number density on the sphere of about 4 μm^{-2}, of the same order as that used in experimental realizations [11]. The (anisotropic) interaction potential reads

$$v_{\rm int}(\mathbf{r}) = v_{\rm HS}(r) + \frac{\mu_0 d_m^2}{4\pi}\frac{1-3\cos^2\theta}{r^3}, \qquad (4)$$

where μ_0 is the vacuum permeability, $d_m = 9.93\mu_B$ is the magnitude of the dipole moment of a ^{164}Dy atom, μ_B is the Bohr magneton, and $\cos\theta = \hat{\mathbf{r}}\cdot\hat{\mathbf{z}}$ [82]. Finally, $v_{\rm HS}(r)$ is the hard-sphere potential with core diameter equal to the scattering length a [51].

We simulate the system for various a, considering values up to $10^3 a_0$, with a_0 the Bohr radius, thus much smaller than the sphere radius taken to be $R = 2.6$ μm (or $R \approx 50 \times 10^3 a_0$). Our results for $N = 360$ and $T = 1$ nK are illustrated in Fig. 4. As is clear from Eq. (4), particles

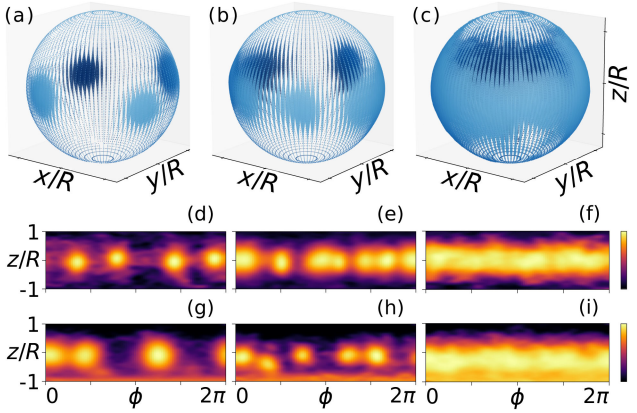

FIG. 4. Dipolar atoms on a sphere. (a)–(c) Particle density for $N = 360$, $T = 1$ nK, and $R = 2.6$ μm, at $a/a_0 = 5$ (a), $a/a_0 = 50$ (b), and $a/a_0 = 350$ (c). The density increases with the size of the points, while colors are a guide for the eye. (d)–(f) Area-preserving projections of the densities in (a)–(c). (g)–(i) Effect of gravity. Brighter colors indicate larger values of the density (log scale).

attract each other along the z direction and repel each other along x and y. As long as a is much smaller than R, particles move away from the poles of the sphere and bunch together around the equator. Indeed, up to $a \approx 150 a_0$, particles form clusters lined up along the equator, as seen in Figs. 4(a) and 4(b). At variance with what is observed for dipolar clusters in trapped Euclidean geometries [36], the cluster phase on the sphere excludes zigzag configurations: In Figs. 4(a) and 4(b), clusters remain on the equator due to the lack of a significant repulsion along z that could counteract the mutual attraction. Unless a is very small, the superfluid fraction for rotations around z is finite and significantly larger than f_s for rotations around x and y, thus qualifying this state as supersolid [Fig. 5(a)] [83]. For

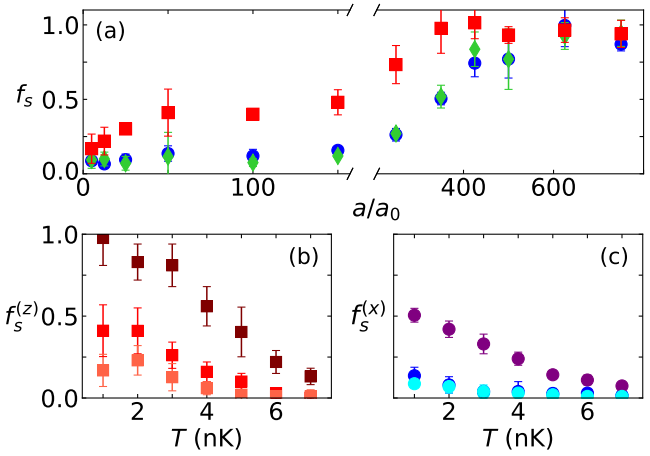

FIG. 5. (a) Superfluid fractions $f_s^{(x)}$ (blue circles), $f_s^{(y)}$ (green diamonds), and $f_s^{(z)}$ (red squares) as a function of a. (b),(c) Thermal behavior of $f_s^{(z)}$ and $f_s^{(x)}$, for $a/a_0 = 5$ (pink and light blue), 50 (red and blue), and 350 (brown and purple).

larger a, due to the increased particle exclusion, clusters grow in size and merge together forming a ribbon wrapped around the sphere; see Figs. 4(c) and 4(f). This specific configuration is consistent with the density profile seen in [26,27]. Beyond $a \approx 200a_0$, the ribbon is homogeneous; however, between $a = 150a_0$ and $a = 200a_0$, there is a wide crossover region where the clusters are still present as azimuthal density modulations. The modulated-to-unmodulated transition is shifted to slightly larger a compared to other trapped geometries (see, e.g., [85] and references cited therein) because of the enhanced stability of spherically confined clusters. The superfluid fraction along z is still significantly larger than in the other directions. Finally, for very large values of $a > 500a_0$, a homogeneous superfluid state emerges, similar to the one shown in Figs. 1(a) and 1(d). Simulations at different values of N but fixed density show no significant scaling, a strong indication that the same supersolid phase persists at larger numbers of particles, up to experimental values. The temperature analysis indicates that the supersolid behaves differently from the superfluid ribbon [see Figs. 5(b) and 5(c)]. In the former case, $f_s^{(z)}$ remains nonzero up to $\approx$5 nK due to a nonzero superfluid signal of the system around z. As for $f_s^{(x)}$, the signal is smaller and substantially constant as a result of the thickness of the supersolid in the latitudinal direction. Instead, the ribbon remains superfluid up to much higher temperatures, while keeping its anisotropic character for all T.

Figures 4(g)–4(i) depict simulations carried out by including the effect of gravity on ^{164}Dy atoms. Interestingly, for small enough a the atoms still form a ring of clusters perpendicular to z, although their center of mass is no longer at $z = 0$, but slightly shifted downward. For larger values of a, even though part of the atoms are found near the south pole, a shifted superfluid ribbon is still evident. This is to be contrasted with what happens when we remove the dipolar component of the interaction, but still keep the hard-core repulsion: In this case, all particles are pushed by gravity to the bottom of the trap [51].

To conclude, we have investigated the equilibrium phases of identical bosons in a shell trap. As the bubble expands, the system switches from three to two dimensional in a continuous fashion. In this peculiar setting, the PIMC algorithm needs an *ad hoc* modification that we have discussed at length in [51]. With this tool at hand, we have considered two species of bosons, i.e., soft-core atoms and dipolar atoms, providing evidence at small nonzero temperature of two unconventional supersolid behaviors. We have argued that the realization of these phases is within reach of present-day technology. Very significantly, we have shown that the dipolar supersolid on the sphere is robust to the effects of gravity. This surprising result indicates that it could be probed experimentally even without sending the apparatus to space. More generally, the ideas underlying our original implementation of the PIMC algorithm on the sphere can profitably be replicated for other curved surfaces, allowing us to gain insight into the peculiarities of bosons in spaces where the geometric potential is nonzero (see more in the last section of [51]).

In this Letter, we have focused on demonstrating the existence of a supersolid phase on the sphere. Using the same numerical techniques, it would be also possible to investigate the nature of the superfluid phase on the sphere, e.g., Berezinskii-Kosterlitz-Thouless behavior or reentrant effects [85,86]. Our work might also be relevant to supersolid phases in the crust of neutron stars [87]. The dynamical properties of shell-trapped bosons are another open problem and an active area of research [88]. For example, it would be interesting to see whether the superfluid ribbon in Figs. 4(c) and 4(f) can support persistent currents in the same way as does a superfluid ring [89–91].

The authors acknowledge the NICIS Centre for High-Perfomance Computing, South Africa, for providing computational resources. M. C. and F. C. acknowledge financial support from PNRR MUR Project No. PE0000023-NQSTI. Fruitful discussions with M. Boninsegni, T. Macrì, A. Mendoza-Coto, G. Modugno, and S. Moroni are gratefully acknowledged.

*matteo.ciardi@tuwien.ac.at
†fabio.cinti@unifi.it
‡giuseppe.pellicane@unime.it
§sprestipino@unime.it

[1] I. Bloch, J. Dalibard, and W. Zwerger, Many-body physics with ultracold gases, Rev. Mod. Phys. **80**, 885 (2008).
[2] I. Bloch, J. Dalibard, and S. Nascimbène, Quantum simulations with ultracold quantum gases, Nat. Phys. **8**, 267 (2012).
[3] B. M. Garraway and H. Perrin, Recent developments in trapping and manipulation of atoms with adiabatic potentials, J. Phys. B **49**, 172001 (2016).
[4] H. Perrin and B. M. Garraway, Trapping atoms with radio frequency adiabatic potentials, in *Advances in Atomic, Molecular, and Optical Physics* (Elsevier, New York, 2017), pp. 181–262.
[5] O. Zobay and B. M. Garraway, Two-dimensional atom trapping in field-induced adiabatic potentials, Phys. Rev. Lett. **86**, 1195 (2001).
[6] O. Zobay and B. M. Garraway, Atom trapping and two-dimensional Bose-Einstein condensates in field-induced adiabatic potentials, Phys. Rev. A **69**, 023605 (2004).
[7] Y. Colombe, E. Knyazchyan, O. Morizot, B. Mercier, V. Lorent, and H. Perrin, Ultracold atoms confined in rf-induced two-dimensional trapping potentials, Europhys. Lett. **67**, 593 (2004).
[8] O. Morizot, C. L. G. Alzar, P.-E. Pottie, V. Lorent, and H. Perrin, Trapping and cooling of rf-dressed atoms in a quadrupole magnetic field, J. Phys. B **40**, 4013 (2007).
[9] T. L. Harte, E. Bentine, K. Luksch, A. J. Barker, D. Trypogeorgos, B. Yuen, and C. J. Foot, Ultracold atoms

in multiple radio-frequency dressed adiabatic potentials, Phys. Rev. A **97**, 013616 (2018).
[10] A. Messiah, *Quantum Mechanics*, Dover Books on Physics (Dover Publications, Newburyport, 2014).
[11] N. Lundblad, R. A. Carollo, C. Lannert, M. J. Gold, X. Jiang, D. Paseltiner, N. Sergay, and D. C. Aveline, Shell potentials for microgravity Bose-Einstein condensates, npj Microgravity **5**, 30 (2019).
[12] D. C. Aveline, J. R. Williams, E. R. Elliott, C. Dutenhoffer, J. R. Kellogg, J. M. Kohel, N. E. Lay, K. Oudrhiri, R. F. Shotwell, N. Yu, and R. J. Thompson, Observation of Bose-Einstein condensates in an Earth-orbiting research lab, Nature (London) **582**, 193 (2020).
[13] R. A. Carollo, D. C. Aveline, B. Rhyno, S. Vishveshwara, C. Lannert, J. D. Murphree, E. R. Elliott, J. R. Williams, R. J. Thompson, and N. Lundblad, Observation of ultracold atomic bubbles in orbital microgravity, Nature (London) **606**, 281 (2022).
[14] Y. Guo, E. M. Gutierrez, D. Rey, T. Badr, A. Perrin, L. Longchambon, V. S. Bagnato, H. Perrin, and R. Dubessy, Expansion of a quantum gas in a shell trap, New J. Phys. **24**, 093040 (2022).
[15] F. Jia, Z. Huang, L. Qiu, R. Zhou, Y. Yan, and D. Wang, Expansion dynamics of a shell-shaped Bose-Einstein condensate, Phys. Rev. Lett. **129**, 243402 (2022).
[16] M. Meister, A. Roura, E. M. Rasel, and W. P. Schleich, The space atom laser: An isotropic source for ultra-cold atoms in microgravity, New J. Phys. **21**, 013039 (2019).
[17] N. S. Móller, F. E. A. dos Santos, V. S. Bagnato, and A. Pelster, Bose-Einstein condensation on curved manifolds, New J. Phys. **22**, 063059 (2020).
[18] A. Tononi and L. Salasnich, Bose-Einstein condensation on the surface of a sphere, Phys. Rev. Lett. **123**, 160403 (2019).
[19] S. J. Bereta, L. Madeira, V. S. Bagnato, and M. A. Caracanhas, Bose-Einstein condensation in spherically symmetric traps, Am. J. Phys. **87**, 924 (2019).
[20] A. Tononi, F. Cinti, and L. Salasnich, Quantum bubbles in microgravity, Phys. Rev. Lett. **125**, 010402 (2020).
[21] A. Tononi, A. Pelster, and L. Salasnich, Topological superfluid transition in bubble-trapped condensates, Phys. Rev. Res. **4**, 013122 (2022).
[22] C. Lannert, T.-C. Wei, and S. Vishveshwara, Dynamics of condensate shells: Collective modes and expansion, Phys. Rev. A **75**, 013611 (2007).
[23] K. Padavić, K. Sun, C. Lannert, and S. Vishveshwara, Physics of hollow Bose-Einstein condensates, Europhys. Lett. **120**, 20004 (2018).
[24] K. Sun, K. Padavić, F. Yang, S. Vishveshwara, and C. Lannert, Static and dynamic properties of shell-shaped condensates, Phys. Rev. A **98**, 013609 (2018).
[25] B. Rhyno, N. Lundblad, D. C. Aveline, C. Lannert, and S. Vishveshwara, Thermodynamics in expanding shell-shaped Bose-Einstein condensates, Phys. Rev. A **104**, 063310 (2021).
[26] P. C. Diniz, E. A. B. Oliveira, A. R. P. Lima, and E. A. L. Henn, Ground state and collective excitations of a dipolar Bose-Einstein condensate in a bubble trap, Sci. Rep. **10**, 4831 (2020).
[27] S. K. Adhikari, Dipolar Bose-Einstein condensate in a ring or in a shell, Phys. Rev. A **85**, 053631 (2012).
[28] F. Cinti and M. Boninsegni, Classical and quantum filaments in the ground state of trapped dipolar Bose gases, Phys. Rev. A **96**, 013627 (2017).
[29] M. Arazo, R. Mayol, and M. Guilleumas, Shell-shaped condensates with gravitational sag: Contact and dipolar interactions, New J. Phys. **23**, 113040 (2021).
[30] S. Eckel, A. Kumar, T. Jacobson, I. B. Spielman, and G. K. Campbell, A rapidly expanding Bose-Einstein condensate: An expanding universe in the lab, Phys. Rev. X **8**, 021021 (2018).
[31] M. F. Hagan and G. M. Grason, Equilibrium mechanisms of self-limiting assembly, Rev. Mod. Phys. **93**, 025008 (2021).
[32] N. Lundblad, D. C. Aveline, A. Balaž, E. Bentine, N. P. Bigelow, P. Boegel, M. A. Efremov, N. Gaaloul, M. Meister, M. Olshanii, C. A. R. S. de Melo, A. Tononi, S. Vishveshwara, A. C. White, A. Wolf, and B. M. Garraway, Perspective on quantum bubbles in microgravity, Quantum Sci. Technol. **8**, 024003 (2023).
[33] T. Lahaye, C. Menotti, L. Santos, M. Lewenstein, and T. Pfau, The physics of dipolar bosonic quantum gases, Rep. Prog. Phys. **72**, 126401 (2009).
[34] G. Biagioni, N. Antolini, A. Alaña, M. Modugno, A. Fioretti, C. Gabbanini, L. Tanzi, and G. Modugno, Dimensional crossover in the superfluid-supersolid quantum phase transition, Phys. Rev. X **12**, 021019 (2022).
[35] L. Chomaz, I. Ferrier-Barbut, F. Ferlaino, B. Laburthe-Tolra, B. L. Lev, and T. Pfau, Dipolar physics: A review of experiments with magnetic quantum gases., Rep. Prog. Phys. **86**, 026401 (2023).
[36] M. A. Norcia, C. Politi, L. Klaus, E. Poli, M. Sohmen, M. J. Mark, R. N. Bisset, L. Santos, and F. Ferlaino, Two-dimensional supersolidity in a dipolar quantum gas, Nature (London) **596**, 357 (2021).
[37] L. Tanzi, E. Lucioni, F. Famà, J. Catani, A. Fioretti, C. Gabbanini, R. N. Bisset, L. Santos, and G. Modugno, Observation of a dipolar quantum gas with metastable supersolid properties, Phys. Rev. Lett. **122**, 130405 (2019).
[38] L. Chomaz, D. Petter, P. Ilzhöfer, G. Natale, A. Trautmann, C. Politi, G. Durastante, R. M. W. van Bijnen, A. Patscheider, M. Sohmen, M. J. Mark, and F. Ferlaino, Long-lived and transient supersolid behaviors in dipolar quantum gases, Phys. Rev. X **9**, 021012 (2019).
[39] F. Böttcher, J.-N. Schmidt, M. Wenzel, J. Hertkorn, M. Guo, T. Langen, and T. Pfau, Transient supersolid properties in an array of dipolar quantum droplets, Phys. Rev. X **9**, 011051 (2019).
[40] A. Browaeys and T. Lahaye, Many-body physics with individually controlled Rydberg atoms, Nat. Phys. **16**, 132 (2020).
[41] N. Henkel, R. Nath, and T. Pohl, Three-dimensional roton excitations and supersolid formation in Rydberg-excited Bose-Einstein condensates, Phys. Rev. Lett. **104**, 195302 (2010).
[42] G. Pupillo, A. Micheli, M. Boninsegni, I. Lesanovsky, and P. Zoller, Strongly correlated gases of Rydberg-dressed atoms: Quantum and classical dynamics, Phys. Rev. Lett. **104**, 223002 (2010).

[43] F. Cinti, P. Jain, M. Boninsegni, A. Micheli, P. Zoller, and G. Pupillo, Supersolid droplet crystal in a dipole-blockaded gas, Phys. Rev. Lett. **105**, 135301 (2010).

[44] J. B. Balewski, A. T. Krupp, A. Gaj, S. Hofferberth, R. Löw, and T. Pfau, Rydberg dressing: Understanding of collective many-body effects and implications for experiments, New J. Phys. **16**, 063012 (2014).

[45] F. Ancilotto, M. Rossi, and F. Toigo, Supersolid structure and excitation spectrum of soft-core bosons in three dimensions, Phys. Rev. A **88**, 033618 (2013).

[46] F. Cinti, T. Macrì, W. Lechner, G. Pupillo, and T. Pohl, Defect-induced supersolidity with soft-core bosons, Nat. Commun. **5**, 3235 (2014).

[47] M. Kunimi and Y. Kato, Mean-field and stability analyses of two-dimensional flowing soft-core bosons modeling a supersolid, Phys. Rev. B **86**, 060510(R) (2012).

[48] S. Prestipino, A. Sergi, and E. Bruno, Freezing of soft-core bosons at zero temperature: A variational theory, Phys. Rev. B **98**, 104104 (2018).

[49] D. M. Ceperley, Path integrals in the theory of condensed helium, Rev. Mod. Phys. **67**, 279 (1995).

[50] M. Boninsegni, Nikolay Prokof'ev, and B. Svistunov, Worm algorithm for continuous-space path integral Monte Carlo simulations, Phys. Rev. Lett. **96**, 070601 (2006).

[51] See Supplemental Material at http://link.aps.org/supplemental/10.1103/PhysRevLett.132.026001 which cites references [52–76], for additional information on the techniques used and results.

[52] R. Feynman, A. Hibbs, and D. Styer, *Quantum Mechanics and Path Integrals*, Dover Books on Physics (Dover Publications, New York, 2010).

[53] M. Boninsegni, Permutation sampling in path integral Monte Carlo, J. Low Temp. Phys. **141**, 27 (2005).

[54] J. Cao and B. J. Berne, A new quantum propagator for hard sphere and cavity systems, J. Chem. Phys. **97**, 2382 (1992).

[55] S. Pilati, S. Giorgini, and N. Prokof'ev, Critical temperature of interacting Bose gases in two and three dimensions, Phys. Rev. Lett. **100**, 140405 (2008).

[56] H. Saito, Path-integral Monte Carlo study on a droplet of a dipolar Bose-Einstein condensate stabilized by quantum fluctuation, J. Phys. Soc. Jpn. **85**, 053001 (2016).

[57] S. A. Chin, Symplectic integrators from composite operator factorizations, Phys. Lett. A **226**, 344 (1997).

[58] M. Ciardi, T. Macrì, and F. Cinti, Finite-temperature phases of trapped bosons in a two-dimensional quasiperiodic potential, Phys. Rev. A **105**, L011301 (2022).

[59] P. Jain, F. Cinti, and M. Boninsegni, Structure, Bose-Einstein condensation, and superfluidity of two-dimensional confined dipolar assemblies, Phys. Rev. B **84**, 014534 (2011).

[60] M. Boninsegni and N. V. Prokof'ev, Colloquium: Supersolids: What and where are they?, Rev. Mod. Phys. **84**, 759 (2012).

[61] A. J. Leggett, Can a solid be "superfluid?", Phys. Rev. Lett. **25**, 1543 (1970).

[62] P. Sindzingre, M. L. Klein, and D. M. Ceperley, Path-integral Monte Carlo study of low-temperature ^{4}He clusters, Phys. Rev. Lett. **63**, 1601 (1989).

[63] A. J. Moreno and C. N. Likos, Diffusion and relaxation dynamics in cluster crystals, Phys. Rev. Lett. **99**, 107801 (2007).

[64] The videos are available on request upon contacting the authors.

[65] Molecular dynamics particle trajectories for the harmonic trap (2023).

[66] Molecular dynamics particle trajectories for the icosahedral distribution of clusters (2023).

[67] L. Kaplan, N. T. Maitra, and E. J. Heller, Quantizing constrained systems, Phys. Rev. A **56**, 2592 (1997).

[68] P. Leboeuf and N. Pavloff, Bose-Einstein beams: Coherent propagation through a guide, Phys. Rev. A **64**, 033602 (2001).

[69] L. Salasnich, A. Parola, and L. Reatto, Effective wave equations for the dynamics of cigar-shaped and disk-shaped Bose condensates, Phys. Rev. A **65**, 043614 (2002).

[70] P. Sandin, M. Ögren, M. Gulliksson, J. Smyrnakis, M. Magiropoulos, and G. M. Kavoulakis, Dimensional reduction in Bose-Einstein condensed clouds of atoms confined in tight potentials of any geometry and any interaction strength, Phys. Rev. E **95**, 012142 (2017).

[71] L. Salasnich, Bose-Einstein condensate in an elliptical waveguide, SciPost Phys. Core **5**, 015 (2022).

[72] G.-H. Liang and M.-Y. Lai, Effective quantum dynamics in curved thin-layer system with inhomogeneous confinement, Phys. Rev. A **107**, 022213 (2023).

[73] H. Jensen and H. Koppe, Quantum mechanics with constraints, Ann. Phys. (N.Y.) **63**, 586 (1971).

[74] R. C. T. da Costa, Quantum mechanics of a constrained particle, Phys. Rev. A **23**, 1982 (1981).

[75] S. Prestipino, A. Laio, and E. Tosatti, Systematic improvement of classical nucleation theory, Phys. Rev. Lett. **108**, 225701 (2012).

[76] P. Hartman and A. Wintner, On the third fundamental form of a surface, Am. J. Math. **75**, 298 (1953).

[77] C. N. Likos, A. Lang, M. Watzlawek, and H. Löwen, Criterion for determining clustering versus reentrant melting behavior for bounded interaction potentials, Phys. Rev. E **63**, 031206 (2001).

[78] S. Prestipino and P. V. Giaquinta, Ground state of weakly repulsive soft-core bosons on a sphere, Phys. Rev. A **99**, 063619 (2019).

[79] T. Macrì, F. Maucher, F. Cinti, and T. Pohl, Elementary excitations of ultracold soft-core bosons across the superfluid-supersolid phase transition, Phys. Rev. A **87**, 061602(R) (2013).

[80] T. Macrì, S. Saccani, and F. Cinti, Ground state and excitation properties of soft-core bosons, J. Low Temp. Phys. **177**, 59 (2014).

[81] S. Franzini, L. Reatto, and D. Pini, Formation of cluster crystals in an ultra-soft potential model on a spherical surface, Soft Matter **14**, 8724 (2018).

[82] M. A. Baranov, Theoretical progress in many-body physics with ultracold dipolar gases, Phys. Rep. **464**, 71 (2008).

[83] We note that, despite this supersolid being quasi-one-dimensional, no supersolid phase exists in the strictly one-dimensional system; see, for instance, Ref. [84].

[84] T. Roscilde and M. Boninsegni, Off-diagonal correlations in a one-dimensional gas of dipolar bosons, New J. Phys. **12**, 033032 (2010).
[85] M. Sohmen, C. Politi, L. Klaus, L. Chomaz, M. J. Mark, M. A. Norcia, and F. Ferlaino, Birth, life, and death of a dipolar supersolid, Phys. Rev. Lett. **126**, 233401 (2021).
[86] J. Sánchez-Baena, C. Politi, F. Maucher, F. Ferlaino, and T. Pohl, Heating a dipolar quantum fluid into a solid, Nat. Commun. **14**, 1868 (2023).
[87] A. Recati and S. Stringari, Supersolidity in ultracold dipolar gases, Nat. Rev. Phys. **5**, 735 (2023).
[88] G. Li and D. K. Efimkin, Equatorial waves in rotating bubble-trapped superfluids, Phys. Rev. A **107**, 023319 (2023).
[89] C. Ryu, M. F. Andersen, P. Cladé, V. Natarajan, K. Helmerson, and W. D. Phillips, Observation of persistent flow of a Bose-Einstein condensate in a toroidal trap, Phys. Rev. Lett. **99**, 260401 (2007).
[90] L. Corman, L. Chomaz, T. Bienaimé, R. Desbuquois, C. Weitenberg, S. Nascimbène, J. Dalibard, and J. Beugnon, Quench-induced supercurrents in an annular Bose gas, Phys. Rev. Lett. **113**, 135302 (2014).
[91] Y. Guo, R. Dubessy, M. d. G. de Herve, A. Kumar, T. Badr, A. Perrin, L. Longchambon, and H. Perrin, Supersonic rotation of a superfluid: A long-lived dynamical ring, Phys. Rev. Lett. **124**, 025301 (2020).